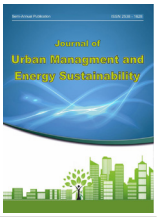
International Journal of Urban Management and Energy Sustainability (IJUMES)

Homepage: http://www.ijumes.com



ORIGINAL RESEARCH PAPER

Numerical Investigation and Seasonal Optimization of a Phase-Change-Material-Integrated Solar Water Heating System

Yahya Tavakolpour, Seyed Amir Abbas Oloomi*, Mohammad Hasan Zare, Seyed Ali Agha Mirjalily, Mohsen Mazidi

Department of Mechanical Engineering, Ya.C, Islamic Azad University, Yazd, Iran

ARTICLE INFO

Article History:
Received 2026-07-01
Revised 2026-09-05
Accepted 2026-10-18

Keywords:
COMSOL Multiphysics; phase change material; seasonal optimization; solar water heating; thermal energy storage

ABSTRACT

Solar water heating is a mature, low-carbon technology for supplying domestic hot water, yet the intermittency of solar radiation creates a persistent mismatch between supply and demand, particularly in buildings with large, time-varying thermal loads. Integrating phase change materials (PCMs) for latent thermal storage can bridge this gap, but the combined influence of PCM type, material fraction, flow rate, and season on performance remains insufficiently characterized; this study therefore develops and optimizes a PCM-integrated flat-plate solar water-heating system for building applications. A three-dimensional computational fluid dynamics model was built in COMSOL Multiphysics, solving the coupled mass, momentum, and energy equations with the effective-specific-heat method for phase change and the P1 radiation model. Two commercial storage materials, RT35HC and paraffin wax, were compared with water at 3% and 6% material fractions and standard and doubled flow rates across the twelve months of the year, using seven indicators: energy requirement, energy-storage performance, harvested energy, PCM melt fraction, valve-opening time ratio, outlet temperature, and overall performance. The findings show that increasing the flow rate enhances convective heat transfer and PCM melting, although excessive flow shortens the residence time for heat transfer to the PCM; water, RT35HC, and paraffin wax display distinct seasonal patterns, with RT35HC performing strongly in the warm months. The conclusion shows that no single material–flow-rate combination is optimal year-round, so PCM selection and flow-rate control should be chosen jointly within a season-dependent operating strategy.

DOI: 10.22034/ijumes.2026.2108559.1419

Running Title: Phase-Change-Material-Integrated Solar Water Heating System

NUMBER OF REFERENCES	NUMBER OF FIGURES	NUMBER OF TABLES
26	21	03

*Corresponding Author:
Email: *Amiroloomi@iau.ac.ir*
Phone: 00989375120607
ORCID: https://orcid.org/0000-0002-2931-4025

INTRODUCTION

Global energy demand continues to rise with population growth, urbanization, and technological development, while the environmental impacts of fossil-fuel use have accelerated the transition toward renewable energy (Shafiee & Topal, 2009; Halmann & Steinberg, 1998; Asafu-Adjaye, 2000; Koroneos et al., 2003). Solar energy is especially attractive for building applications because it can supply low- and medium-temperature heat for domestic hot water and space heating, and its potential and diverse solar-thermal applications are well established (Kannan & Vakeesan, 2016; Kabir et al., 2018; Alamdari et al., 2013; Badar Hayat et al., 2019; Wang et al., 2021; Tsalikis & Martinopoulos, 2015; Al Hariri et al., 2024). Solar water heating (SWH) is a mature solar-thermal technology, but its performance is inherently constrained by the temporal variability of solar radiation (Jamar et al., 2016): solar heat is available mainly during daylight, whereas hot-water demand continues through the night and often peaks when solar input is low. Thermal energy storage is therefore essential for the continuity and reliability of solar-assisted heating. Phase change materials (PCMs) provide an attractive latent-heat storage mechanism, absorbing or releasing large quantities of energy within a narrow temperature interval during phase transition, thereby increasing storage density and extending useful operation beyond sunshine hours. Previous investigations have examined PCM placement, collector configuration, fins and metallic strips, porous media, cascaded units, nanofluid enhancement, and different climatic conditions (Hussein et al., 2018; Farahani et al., 2021; Huang et al., 2020; Ding et al., 2020; Khodadadi et al., 2021; Tripathi et al., 2023; Abdellatif et al., 2025; Lenka et al., 2026). Comparable system-level studies have compared thermosyphon solar water heaters (Koua et al., 2020), paraffin-based latent storage coupled with flat-plate collectors (Senthil et al., 2020), photovoltaic-thermal PCM collectors under varying irradiance and flow (Aziz et al., 2023), PCM melting in vertical thermal storage (Senthil et al., 2021), and paraffin-PCM solar heating for residential comfort (Quispe et al., 2026).

Although these studies collectively demonstrate the potential of PCM integration, they typically vary only one or two design parameters and do not fully resolve the interaction among material selection, material fraction, flow rate, and seasonal operating conditions for the configuration examined here. The objective of this study is therefore to numerically characterize and optimize a flat-plate solar water-heating system integrated with RT35HC and paraffin wax, simultaneously considering 3% and 6% material fractions, standard and doubled flow rates, and twelve monthly operating conditions.

MATERIALS AND METHODS

System configuration

The investigated system is a closed-loop forced-circulation solar water-heating system. Its main components are a flat-plate collector, storage tank, circulation piping, pump, measurement devices, supporting structure, galvanized sheets, and thermal insulation. Water is circulated through the collector, receives solar-derived thermal energy, and transfers the collected heat to the storage section.

Flat-plate collector

The numerical model uses the SUN 600.20 flat-plate collector with a nominal area of approximately 2.0 m² and a tilt angle of 45°.

Table 1: Absorption coefficient, emissivity, and thickness of various layers

Layer	Transmissivity	Absorptivity	Emissivity	Thickness (mm)
Glass	0.91	0.005	0.94	3.2
Ethylene Vinyl Acetate (EVA)	0.93	0.005	-	0.5
PV units	0.09	0.8	-	0.3

Bottom surface	0.91	0.005	-	0.5
Mirror	0.95	0.95	-	-

The collector specifications used in the model include an aperture area of 1.92 m², a height of 1730 mm, a depth of 73 mm, a fluid capacity of approximately 28 kg, a zero-loss efficiency of 0.77, an overall heat-transfer coefficient of 4.80 W/(m²·K), a maximum working pressure of 10 bar, and a recommended flow rate of 25 L/(h·m² aperture).

Table 2: Geometric and thermal specifications

Parameter	Unit	SUN 600.20
Total area	m²	2.02
Aperture area	m²	1.92
Overall height	mm	1730
Overall width (with connections)	mm	1170–1215
Depth	mm	73
Fluid capacity	kg	28
Connections	mm	4 × 22
First-order coefficient	W/(m²·K²)	3.745
Second-order coefficient	W/(m²·K²)	0.015
Zero-loss efficiency	-	0.77
Overall heat transfer coefficient	W/(m²·K)	4.80
Maximum working pressure	bar	10
Stagnation temperature	°C	197
Recommended flow rate	l/(h·m² aperture)	25
Tilt angle range	°	15° to 75°
Maximum wind speed	km/h	150
Maximum snow load	kN/m²	0.75

Storage tank and design basis and Governing equations

The design basis considers an 80-gallon (approximately 300 L) storage tank for four persons, with a target hot-water supply temperature of 60°C. A collector area of approximately 2 m² is adopted in accordance with the design guideline used in the original study and the climatic conditions considered for Yasuj city in Iran. The model solves the three-dimensional conservation equations for mass, momentum, and energy. Temperature-dependent density is considered in the fluid formulation. The governing equations are the continuity equation, the momentum equation with viscous stress, and the energy equation including conductive and convective heat transfer.

Radiative heat transfer is represented using the P1 radiation model. The thermal properties of the working and storage materials are incorporated into the energy equation. For the nanofluid formulation reported in the original model, effective density, heat capacity, thermal conductivity, and viscosity are evaluated as functions of the dispersed-material fraction.

$$\partial\rho/\partial t+\nabla.j=\sigma \quad (1)$$

$$\rho(u.\nabla)u=\nabla.[-\rho l+\kappa]+F \quad (2)$$

$$\kappa=\mu(\nabla u+(\nabla u)^{T})-2/3\ \mu(\nabla.u)l \quad (3)$$

$$\rho C_p\ dT/dt+\rho C_p\ u.\nabla T=k\nabla^2\ T+ \quad (4)$$

$$\nabla.(-D_{p1}\nabla G)-\kappa(G-4\pi I_b)=0 \quad (5)$$

$$D_{p1}=1/3(\kappa+\sigma_s) \quad (6)$$

$$\rho_nf=(1-\phi)\,\rho_b+\rho_{np}\,\phi \quad (7)$$

$$(C_p)_{nf}=((1-\phi)\,(C_p\,\rho)_b+(C_p\,\rho)_nP\,\phi)/\rho_{nf} \quad (8)$$

$$k_{nf}/k_b=(2k_b+k_p\,2(k_p-k_b)\phi)/-(k_p-k_b)\phi+2k_b+k_p \quad (9)$$

$$\mu_{nf}=(1_\phi)^{-2.5}\,\mu_b O \quad (10)$$

$$C_{ps}=2.5+174/3(flc2hs(T-313,0.2)-flc2hs(T-316,0.2)) \quad (11)$$

Thermophysical properties

The investigated thermal-storage materials are RT35HC and paraffin wax. The reported properties are: RT35HC density 804.55 kg/m³, specific heat 3550 J/(kg·K), thermal conductivity 0.4 W/(m·K), melting temperature approximately 35°C, and latent heat 220 kJ/kg; paraffin wax density 900 kg/m³, specific heat 2500 J/(kg·K), thermal conductivity 0.21 W/(m·K), melting range approximately 313–316 K, and latent heat 174 kJ/kg. Aluminum oxide is also listed in the original model with a density of 3970 kg/m³, specific heat of 765 J/(kg·K), and thermal conductivity of 40 W/(m·K).

The phase-change process is represented by the effective-specific-heat method. Latent heat is incorporated by modifying the apparent heat capacity within the melting interval. This approach enables the latent heat contribution to be included directly in the transient energy equation.

Table 3. Thermophysical properties of nanoparticles.

Nanoparticles	Density (kg/m³)	Specific Heat (J/(kg·K))	Thermal Conductivity (W/(m·°C))	μ	Melting Point (°C)	Latent Heat of Fusion (J/kg)
Aluminum Oxide (Al_2O_3)	3970	765	40	-	-	-
RT-35HC	804.55	3550	0.4	0.0044	35	220,000
Paraffin Wax	900	2500	0.21	-	313–316	174,000

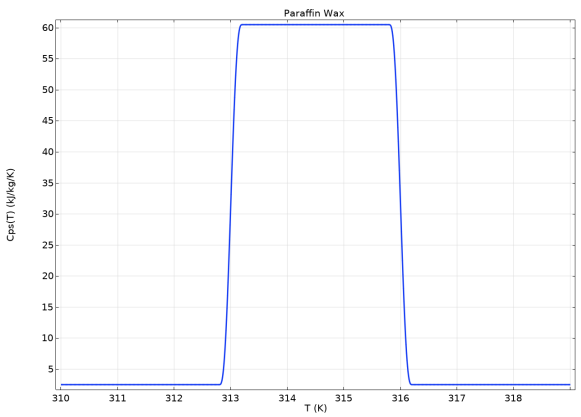


Figure 1: Modified specific heat (Cp) of paraffin wax.

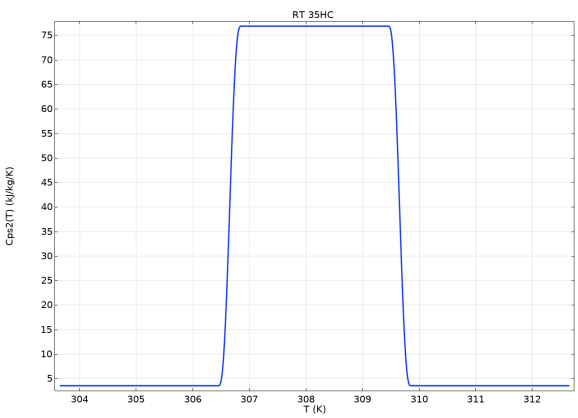


Figure 2: Modified specific heat (Cp) of RT-35HC.

Geometry and boundary conditions

The modeled storage geometry consists of a cylindrical tank approximately 2 m long, with an outer radius of 230 mm and an inner water-flow radius of 50 mm. Twenty copper fins are embedded in the PCM region. The external walls are treated as thermally insulated, no-slip conditions are applied at solid walls, and fully developed flow is assumed at the inlet and outlet. The inlet fluid temperature is set equal to the ambient temperature.

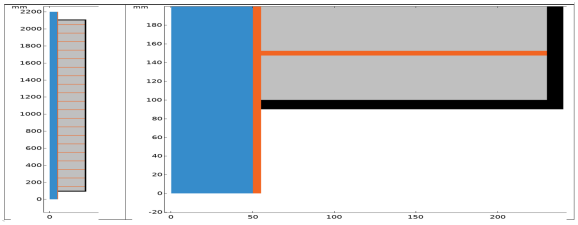


Figure 3: Schematic representation of the problem.

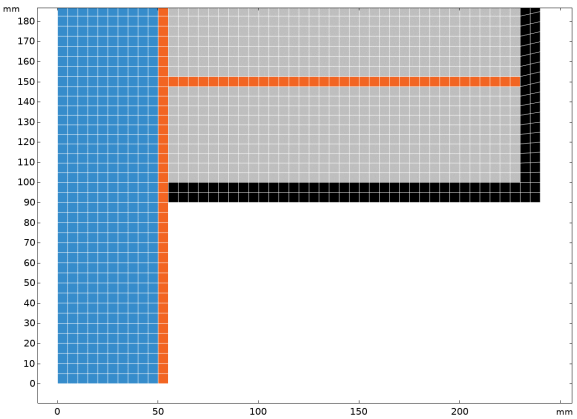


Figure 4: Meshing of the geometry under investigation.

Mesh independence and validation

Three meshes containing 13,686, 19,836, and 29,994 elements were tested. The stored-energy results were nearly identical for the three meshes; therefore, the 19,836-element mesh was selected as a compromise between numerical accuracy and computational cost.

For validation, the simulated collector efficiency under the nominal conditions specified in the original study was compared with the collector catalogue value. The simulation yielded approximately 33%, in close agreement with the reported catalogue value of approximately 33%. This comparison supports the numerical implementation, while the limited validation dataset should be recognized as a limitation of the present study.

FINDINGS AND DISCUSSION

Grid independence and Effect of flow rate on heat transfer and PCM melting

The grid-independence analysis demonstrates negligible differences in the calculated stored-energy response among the three tested meshes.

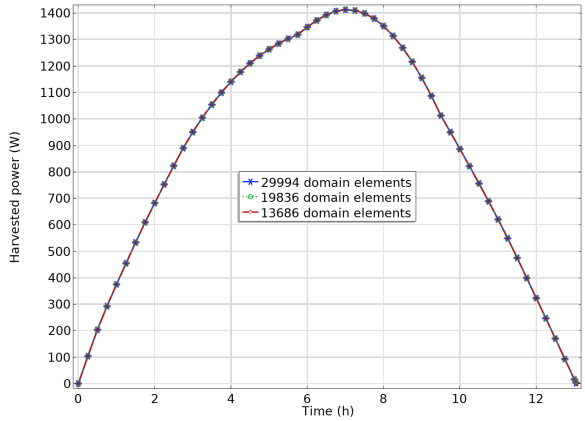


Figure 5: Variations of stored energy for different element counts.

The selected 19,836-element mesh therefore provides a suitable computational resolution for the subsequent parametric simulations. Increasing the inlet velocity increases the convective heat-transfer coefficient and consequently enhances the rate of heat exchange between the circulating fluid and the PCM. The simulations show that the PCM melt fraction increases with flow rate for both paraffin wax and RT35HC. However, the higher velocity also reduces the residence time of the fluid in the heat-transfer region. Consequently, an increase in flow rate does not necessarily translate into a proportional increase in outlet temperature or useful heat transferred to the PCM. This interpretation is consistent with the flow-rate and PCM effects reported in related IJRED solar-thermal studies. The results indicate that flow-rate optimization is a trade-off between stronger convection and shorter residence time. This interaction is important when selecting the operating point for a PCM-integrated solar thermal system.

Seasonal energy requirement

The annual analysis shows substantial seasonal variation in the energy requirement. During warmer months, the available solar energy can exceed the instantaneous thermal demand, creating an opportunity for latent-heat storage. During colder periods, the energy demand increases and the solar contribution becomes

more constrained. Increasing the flow rate to twice the standard value generally improves the reported system performance in the investigated configurations. The results therefore support a seasonal rather than fixed operating strategy. The preferred thermal-storage material and flow rate depend on the thermal conditions prevailing during each period of the year.

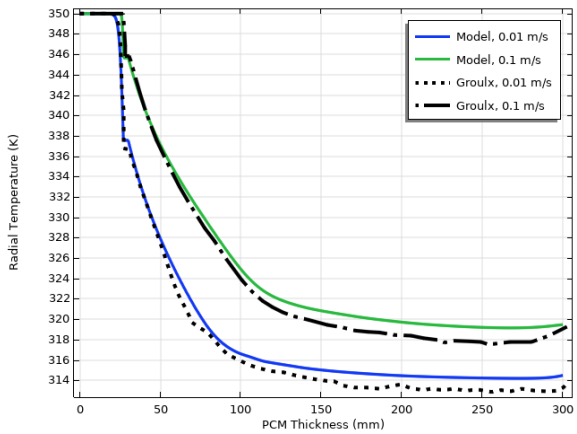


Figure 6: Radial temperature distribution in PCM for different inlet water velocities.

Seasonal energy requirement

The annual analysis shows substantial seasonal variation in the energy requirement. During warmer months, the available solar energy can exceed the instantaneous thermal demand, creating an opportunity for latent-heat storage. During colder periods, the energy demand increases and the solar contribution becomes more constrained. Increasing the flow rate to twice the standard value generally improves the reported system performance in the investigated configurations. The results therefore support a seasonal rather than fixed operating strategy. The preferred thermal-storage material and flow rate depend on the thermal conditions prevailing during each period of the year.

Energy-storage performance

RT35HC at twice the standard flow rate exhibits strong energy-storage performance during the warmer part of the year, particularly around months six to eight. In comparison, paraffin wax at standard flow rate exhibits lower stored-energy performance during the first four months. These differences are associated with the distinct melting temperatures, specific heats, and latent heats of the materials.

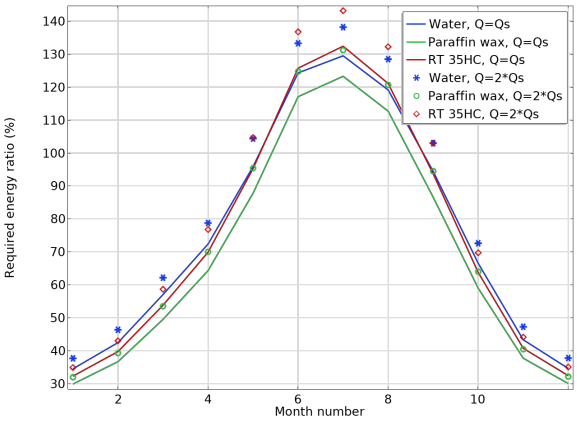


Figure 7: Energy requirement ratio for different months of the year.

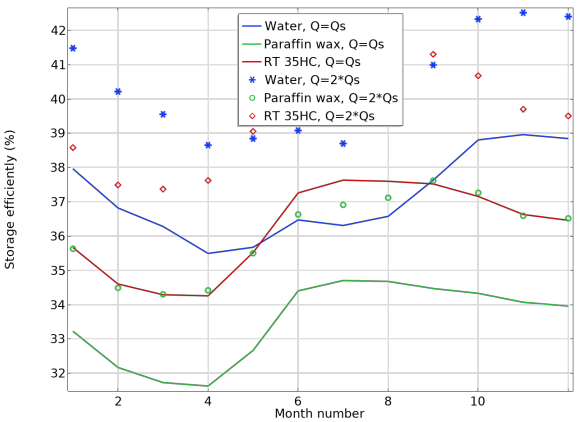


Figure 8: shows the variations in stored energy efficiency during different months of the year.

Energy harvested for a four-person household

The annual analysis for a four-person household indicates that electricity consumption varies considerably with the season. During the sixth month, the original simulation reports approximately 50 kWh of electricity consumption. Under the RT35HC configuration, approximately 13 kWh is reported, while the paraffin-wax configuration reports approximately 12 kWh. These

values correspond to lower electricity demand relative to the stated monthly consumption in the simulated cases. Because these results depend on the specific load assumptions and simulation boundary conditions, they should be interpreted as model-based comparative results rather than direct predictions of field electricity consumption.

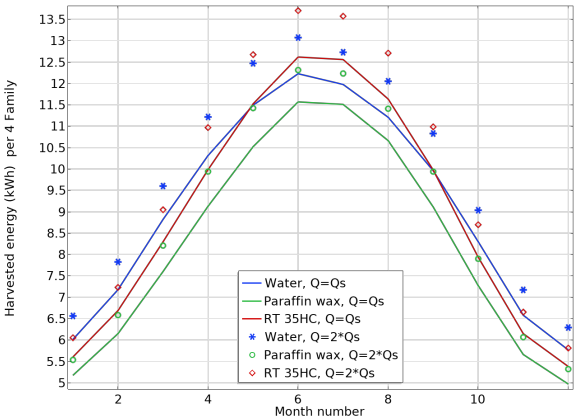


Figure 9: Energy harvested by a household for various months of the year.

PCM melt fraction

The PCM melt fraction increases during the warmer months as a result of higher ambient temperature and solar availability. RT35HC reaches its highest melt fraction during approximately months six to eight. The seasonal behavior confirms that PCM selection should be matched to the operating-temperature range of the solar thermal system. Similar emphasis on PCM melting behavior as a performance indicator has been reported for solar thermal storage systems in IJRED.

Valve-opening time ratio

The valve-opening time ratio varies with both PCM type and month. RT35HC reaches values close to 96% during months six to eight and approximately 91% during the first three months. Paraffin wax reaches approximately 89% in the second month and approximately 93.5% in month eight. The differences are consistent with the distinct melting characteristics of the two PCMs and their interaction with seasonal operating temperatures.

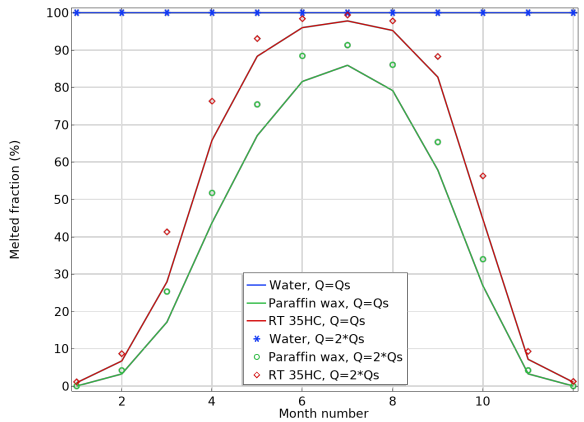


Figure 10: Melt fraction for different months of the year.

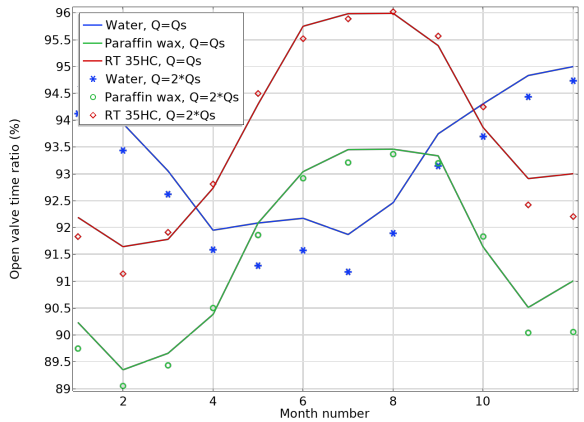


Figure 11: Valve opening time ratio for different months of the year.

Overall system performance

The calculated overall performance varies substantially with material and flow rate. Paraffin wax at standard flow rate produces values of approximately 23–25% during the first four months, whereas doubling the flow rate increases the reported performance to approximately 28–28.5% during months eight to ten. RT35HC at standard flow rate reaches approximately 28–28.5% during months six to nine, while doubling its flow rate produces approximately 30.5–31.5% during months seven to ten. Water at twice the standard flow rate exceeds 31% during the final three months. These results demonstrate that no single material-flow-rate combination is

uniformly optimal throughout the year. Instead, performance is strongly seasonal, and the selection of PCM should be coupled with the expected operating temperature and flow conditions.

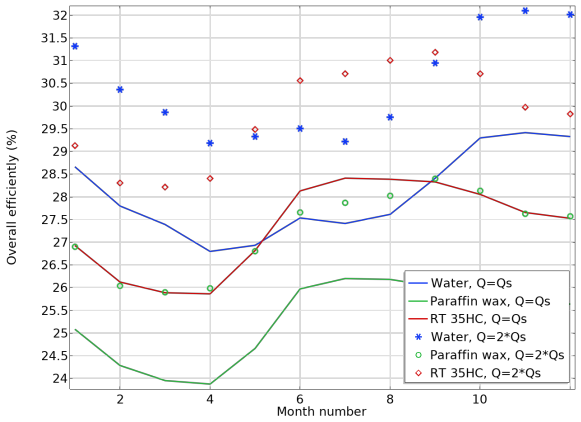
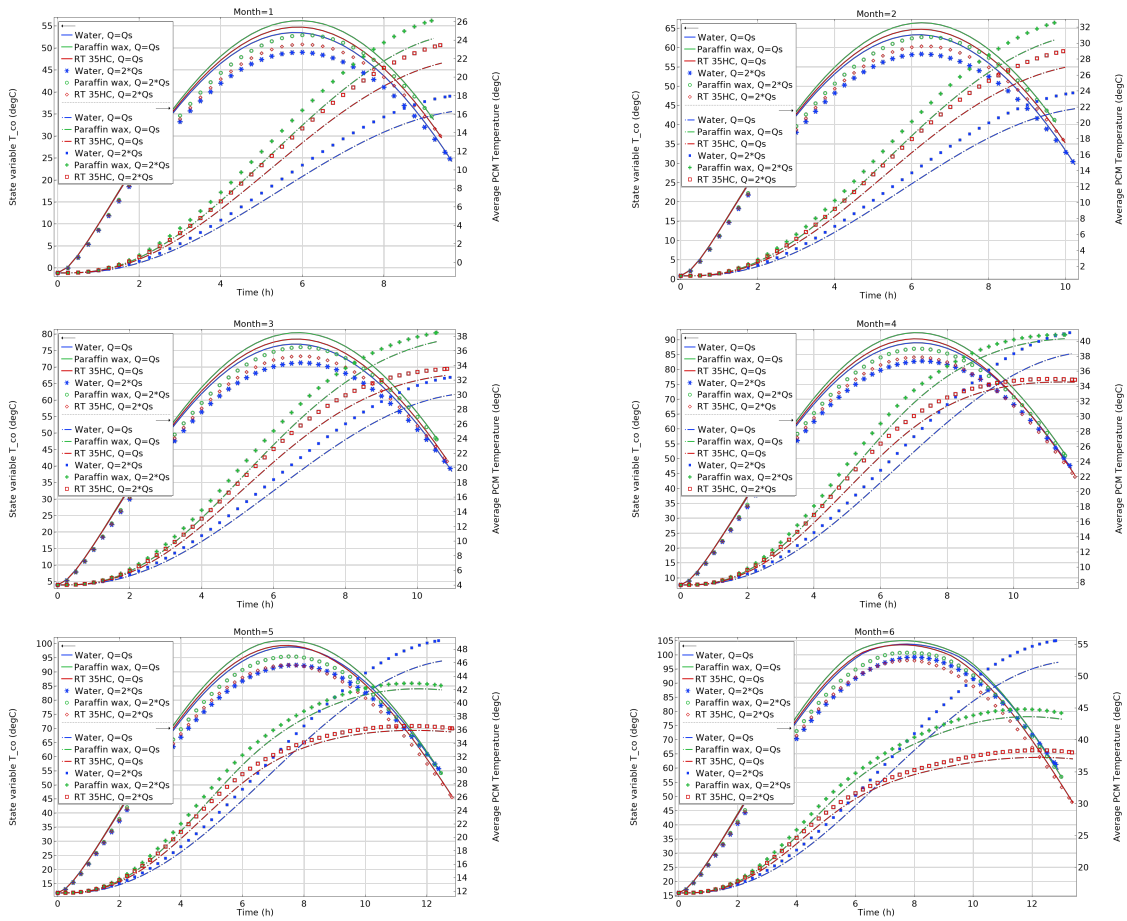


Figure 12: Variations in overall efficiency for different months of the year

Outlet temperature

The collector outlet temperature varies approximately from 26°C to 58°C over the simulated year. During months six to eight, outlet temperatures above 55°C are obtained. Paraffin wax at standard flow rate reaches nearly 58°C in month seven, whereas the lowest outlet temperatures occur for paraffin wax under the same conditions in months one and twelve. For the average PCM temperature, water at twice the standard flow rate performs strongly during months five to nine, with reported values between approximately 46°C and 58°C. During the first four and final three months, paraffin wax at twice the standard flow rate shows the higher reported average PCM temperature, approximately 26–40°C.



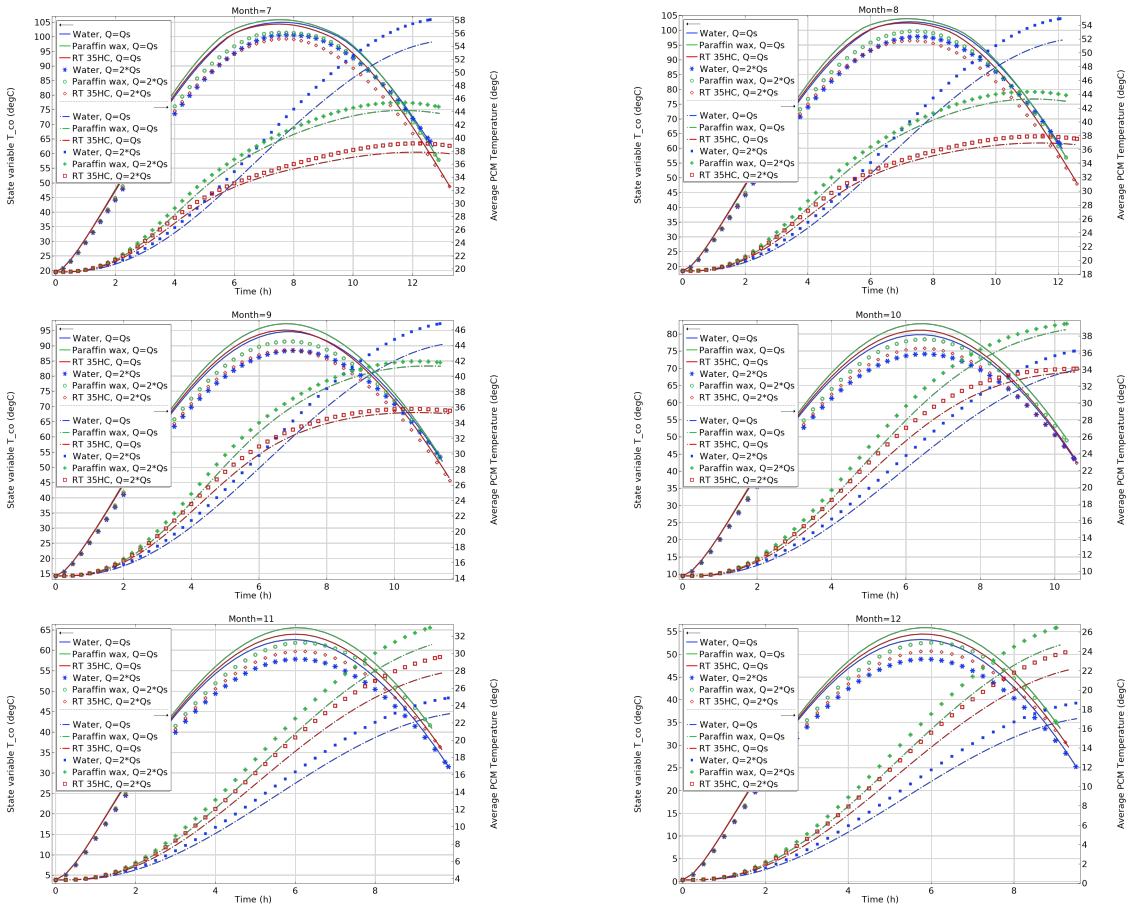


Figure 13: Outlet temperature variations for different months of the year.

Temperature contours

The water temperature contours show similar spatial patterns at the two investigated flow rates, with the highest temperatures occurring near the hot-water flow region. Doubling the flow rate increases convective heat transfer and produces higher average outlet temperature. The reported average outlet temperature at doubled flow rate is approximately 74.5°C for the water case.

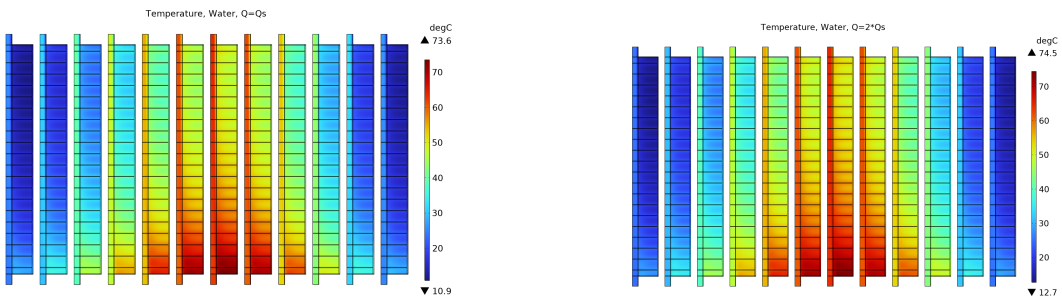


Figure 14: Variations in water temperature contour at different flow rates.

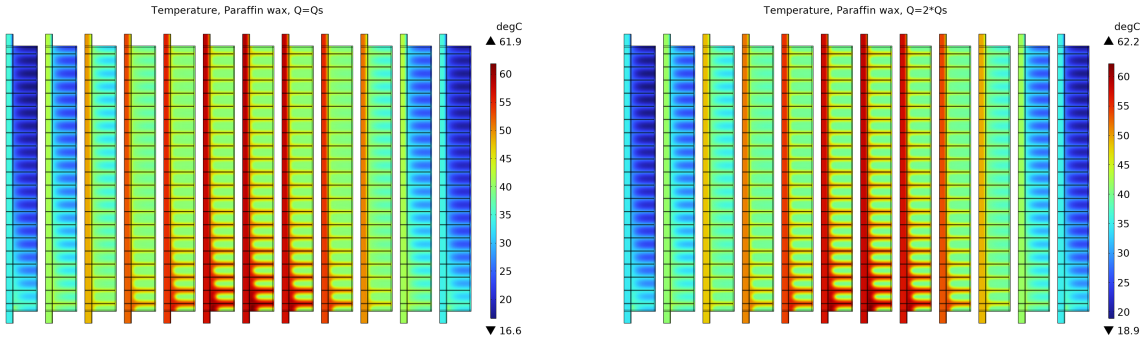


Figure 15: Variations in the temperature contour of paraffin wax at different flow rates.

For paraffin wax, the average outlet temperature at doubled flow rate is approximately 62.2°C, while the corresponding value for RT35HC is approximately 58.4°C. The minimum water temperature is reported to increase by approximately 1.8°C, 2.3°C, and 2.4°C for the water, paraffin-wax, and RT35HC cases, respectively, when the flow rate is doubled.

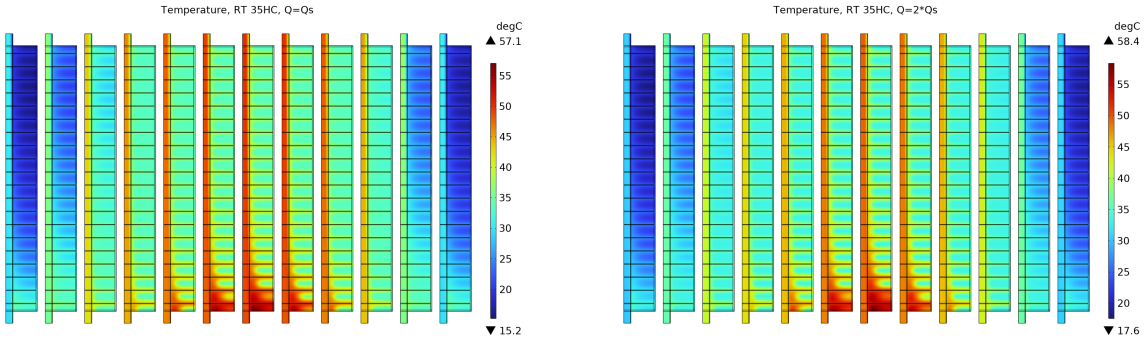


Figure 16: Changes in the temperature contour of RT-35HC for various flow rates.

Effect of material fraction

For the water-based cases, the second month produces a reported efficiency of approximately 55% at a 6% fraction and standard flow rate. During the three summer months, the 6% fraction at twice the standard flow rate produces reported efficiencies of approximately 35–48%. During the final three months, the same configuration remains within approximately 40–50%.

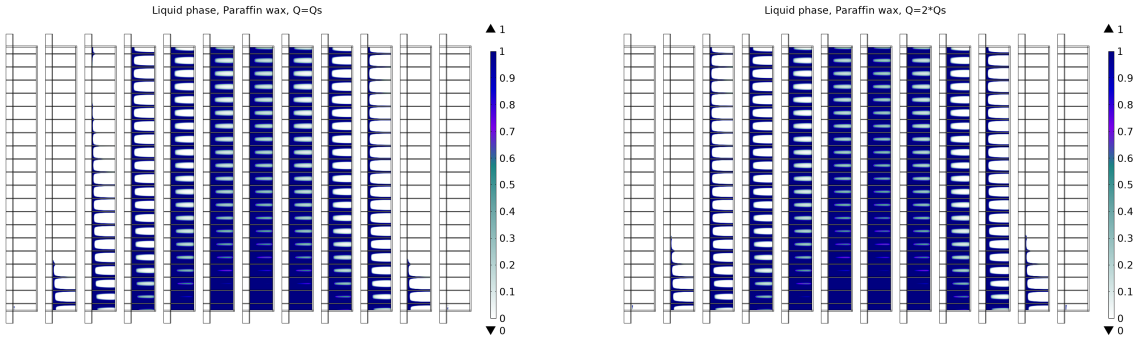


Figure 17: Variations in the melting fraction of paraffin wax at different flow rates.

For RT35HC, the 6% fraction at twice the standard flow rate reaches approximately 85% in the second month and approximately 82–85% during the summer period. During the final three months, the reported range is approximately 65–82%.

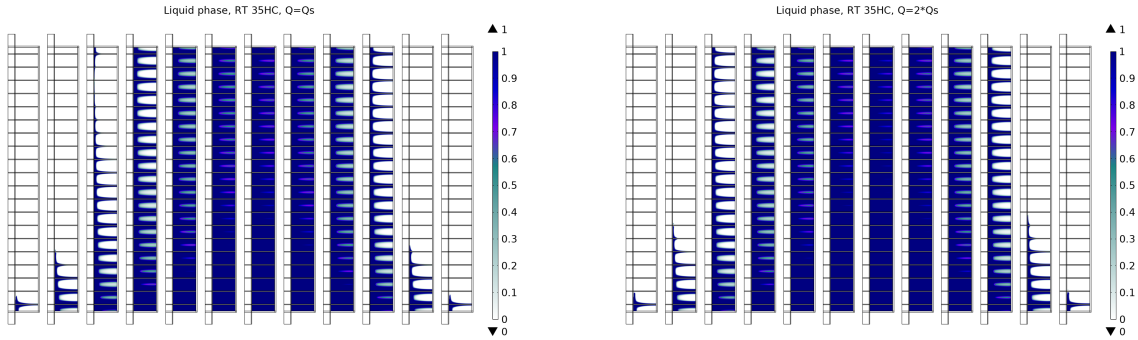


Figure 18: Variations in the melting fraction of RT-35HC at different flow rates.

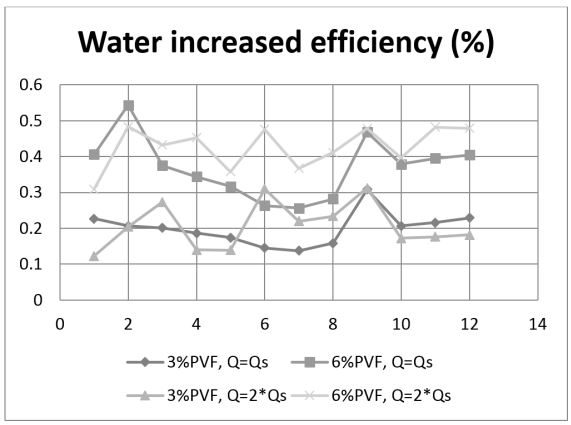


Figure 19: Efficiency variations of water as the working fluid at different weight percentages and flow rates.

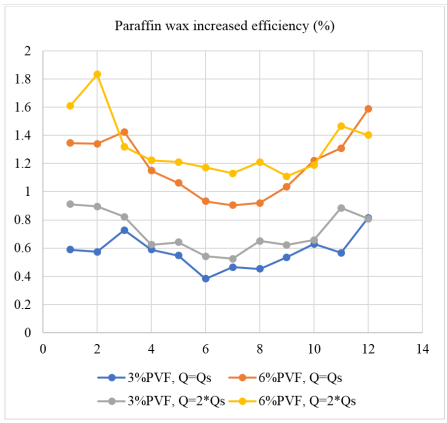


Figure 20: Efficiency variations of paraffin wax at different weight percentages and flow rates.

For paraffin wax, the model reports a performance metric approaching 180% for the 6% fraction at twice the standard flow rate in the second month, with values of approximately 120–160% reported during the final three months at standard flow rate. Because a conventional thermal efficiency defined as useful thermal output divided by incident solar energy cannot physically exceed 100%, these values should be interpreted only according to the exact performance definition used in the original model. The underlying equation, normalization, and units must be verified before the metric is described as 'thermal efficiency' in the final submission. The combined results indicate that the PCM type and material fraction should be selected together with the operating flow rate and season; a single year-round setting may not provide the best thermal response.

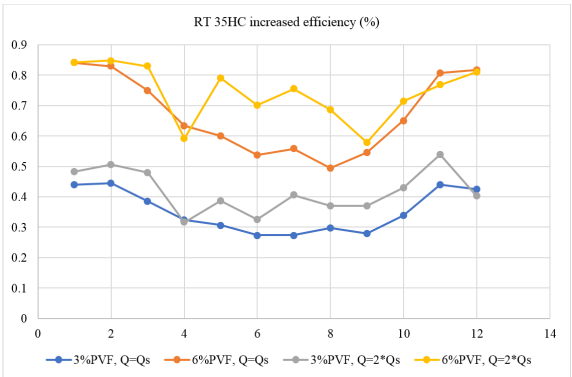


Figure 21: Efficiency variations of RT-35HC at different weight percentages and flow rates.

RESULTS AND CONCLUSION

This study numerically investigated a PCM-integrated flat-plate solar water-heating system for building applications using COMSOL Multiphysics. The analysis considered two commercial PCMs, RT35HC and paraffin wax, different material fractions, two flow-rate conditions, and twelve months of operation. The results demonstrate that flow rate has a strong influence on convective heat transfer and PCM melting. Increasing the flow rate generally increases the convective heat-transfer coefficient and melt fraction, but the reduced residence time can limit the heat transferred to the PCM. The thermal response is therefore governed by a balance between convection intensity and residence time. The seasonal analysis demonstrates that the relative performance of water, RT35HC, and paraffin wax changes over the year. RT35HC shows strong performance during warm-season operation, while paraffin wax also exhibits favorable behavior under several high-temperature conditions. The outlet-temperature analysis further confirms that the material melting range must be compatible with the operating temperature of the solar thermal system.

The principal contribution of the work is the simultaneous assessment of material type, material fraction, flow rate, and seasonal variation within one numerical framework. This integrated approach provides a practical basis for developing season-dependent operating strategies rather than relying on a single fixed design condition. The principal also contributions of this work can be summarized as follows. First, the study integrates PCM type, material fraction, flow rate, and twelve-month seasonal variation within a single unified numerical framework, rather than optimizing these parameters in isolation. Second, two commercial PCMs-RT35HC and paraffin wax are directly compared under identical solar-water-heating conditions, enabling a transparent seasonal contrast of their thermal responses. Third, the results demonstrate that the preferred operating condition shifts with the month, providing a practical basis for season-dependent PCM and flow-rate selection. Fourth, system behavior is assessed through seven complementary performance indicators energy requirement, energy storage, harvested energy, melt fraction, valve-opening time, outlet temperature, and overall performance rather than a single efficiency value. Fifth, the analysis is linked to a four-person hot-water demand and a 300-L storage tank, offering an engineering-scale context for interpreting the thermal-storage results. Taken together, these contributions move beyond single-parameter optimization and establish a season-dependent, multi-indicator design strategy for PCM-integrated solar water-heating systems in high-rise buildings. The findings provide practical guidance for engineers and designers seeking to select the most suitable PCM type and flow rate under varying seasonal conditions, while also highlighting the importance of verifying the exact definition of the reported performance metric exceeding 100% before it is interpreted as a conventional thermal efficiency. Future work should include experimental validation under multiple operating conditions, uncertainty analysis, economic assessment, and a more comprehensive annual energy/exergy evaluation. These extensions would strengthen the practical applicability of the numerical findings.

REFERENCES

Abdellatif, H. E., Belaadi, A., Arshad, A., & Bourchak, M. (2025). Modeling and performance analysis of phase change materials in advanced thermal energy storage systems: A comprehensive review. Journal of Energy Storage, 121, 116517. https://doi.org/10.1016/j.est.2025.116517

Al Hariri, A. H., Khalifa, A. E., & Alawad, S. M. (2024). Techno-economic analysis of solar-powered membrane distillation system with circulated permeate gap. Solar Energy, 267, 112243.

Alamdari, P., Nematollahi, O., & Alemrajabi, A. A. (2013). Solar energy potentials in Iran: A review. Renewable and Sustainable Energy Reviews, 21, 778–788. https://doi.org/10.1016/j.rser.2012.12.052

Asafu-Adjaye, J. (2000). The relationship between energy consumption, energy prices and economic growth: Time series evidence from Asian developing countries. Energy Economics, 22(6), 615–625.

Aziz, M. S. B., Ibrahim, A., & Ishak, M. A. A. B. (2023). Energy performance evaluation of a photovoltaic thermal phase change material (PVT-PCM) using a spiral flow configuration. International Journal of Renewable Energy Development, 12(5), 952–958. https://doi.org/10.14710/ijred.2023.56052

Badar Hayat, M., Ali, D., Cathrine Monyake, K., Alagha, L., & Ahmed, N. (2019). Solar energy—A look into power generation, challenges, and a solar-powered future. International Journal of Energy Research, 43(3), 1049–1067. https://doi.org/10.1002/er.4252

Ding, Z., Wu, W., Chen, Y., & Li, Y. (2020). Dynamic simulation and parametric study of solar water heating system with phase change materials in different climate zones. Solar Energy, 205, 399–408. https://doi.org/10.1016/j.solener.2020.05.075

Farahani, S. D., Farahani, A. D., & Oraki, P. (2021). Improving thermal performance of solar water heater using phase change material and porous material. Heat Transfer Research, 52(16), 69–86. https://doi.org/10.1615/HeatTransRes.2021039550

Halmann, M. M., & Steinberg, M. (1998). Greenhouse gas carbon dioxide mitigation: Science and technology. CRC Press.

Huang, H., Xiao, Y., Lin, J., Zhou, T., Liu, Y., & Zhao, Q. (2020). Improvement of the efficiency of solar thermal energy storage systems by cascading a PCM unit with a water tank. Journal of Cleaner Production, 245, 118864. https://doi.org/10.1016/j.jclepro.2019.118864

Hussein, A., Abd-Elhady, M. S., El-Sheikh, M. N., & El-Metwally, H. T. (2018). Improving heat transfer through paraffin wax by using fins and metallic strips. Arabian Journal for Science and Engineering, 43, 4433–4441. https://doi.org/10.1007/s13369-017-2923-2

Jamar, A., Majid, Z. A. A., Azmi, W. H., Norhafana, M., & Razak, A. A. A. (2016). Review of water heating system for solar energy applications. International Communications in Heat and Mass Transfer, 76, 178–187. https://doi.org/10.1016/j.icheatmasstransfer.2016.05.028

Kabir, E., Kumar, P., Kumar, S., Adelodun, A. A., & Kim, K.-H. (2018). Solar energy: Potential and future prospects. Renewable and Sustainable Energy Reviews, 82(1), 894–900. https://doi.org/10.1016/j.rser.2017.09.094

Kannan, N., & Vakeesan, D. (2016). Solar energy for future world: A review. Renewable and Sustainable Energy Reviews, 62, 1092–1105. https://doi.org/10.1016/j.rser.2016.05.022

Khodadadi, M., Farshad, S. A., Ebrahimpour, Z., & Sheikholeslami, M. (2021). Thermal performance of nanofluid with employing of NEPCM in a PVT-LFR system. Sustainable Energy Technologies and Assessments, 47, 101340. https://doi.org/10.1016/j.seta.2021.101340

Koroneos, C., Spachos, T., & Moussiopoulos, N. (2003). Exergy analysis of renewable energy sources. Renewable Energy, 28(2), 295–310.

Koua, B. K., Koffi, P. M. E., & Gbaha, P. (2020). Comparative study of the thermal performance of two thermosyphon solar water heater systems. International Journal of Renewable Energy Development, 9(3), 401–410. https://doi.org/10.14710/ijred.2020.30575

Lenka, B. C., Shajahan, M. I., Suresh, S., & Bharathiraja, R. (2026). Enhancing thermal and exergy efficiency of flat plate solar collectors using GR42 microencapsulated phase change material. Energy Conversion and Management, 350, 120918. https://doi.org/10.1016/j.enconman.2025.120918

Quispe, K. J., Balboa, O. C., Morales, O. M., García, J. O., & Vilca, H. D. C. (2026). Radiator-type solar heating system with phase change material for residential thermal comfort. International Journal of Renewable Energy Development, 15(1), 106–121. https://doi.org/10.61435/ijred.2026.61348

Senthil, R., Patel, A., Rao, R., & Ganeriwal, S. (2020). Melting behavior of phase change material in a solar vertical thermal energy storage with variable length fins added on the heat transfer tube surfaces. International Journal of Renewable Energy Development, 9(3), 361–367. https://doi.org/10.14710/ijred.2020.29879

Senthil, R., Patel, A., Rao, R., & Ganeriwal, S. (2021). Effect of fluid flow direction on charging of mul-

titube thermal energy storage for flat plate solar collectors. International Journal of Renewable Energy Development, 10(2), 365–371. https://doi.org/10.14710/ijred.2021.34931

Shafiee, S., & Topal, E. (2009). When will fossil fuel reserves be diminished? Energy Policy, 37(1), 181–189.

SUN flat-plate solar collector (model SUN 600.20): Technical specifications [Manufacturer datasheet]. (n.d.). [Source cited as [27] and [28] in Tables 1–2; full publication details to be confirmed by the author.]

Tripathi, B. M., Shukla, S. K., & Rathore, P. K. S. (2023). A comprehensive review on solar to thermal energy conversion and storage using phase change materials. Journal of Energy Storage, 72, 108280. https://doi.org/10.1016/j.est.2023.108280

Tsalikis, G., & Martinopoulos, G. (2015). Solar energy systems potential for nearly net zero energy residential buildings. Solar Energy, 115, 743–756. https://doi.org/10.1016/j.solener.2015.03.037

Wang, P., Liu, Z., & Zhang, L. (2021). Sustainability of compact cities: A review of inter-building effect on building energy and solar energy use. Sustainable Cities and Society, 72, 103035. https://doi.org/10.1016/j.scs.2021.103035

COPYRIGHTS

©2023 The author(s). This is an open access article distributed under the terms of the Creative Commons Attribution (CC BY 4.0), which permits unrestricted use, distribution, and reproduction in any medium, as long as the original authors and source are cited. No permission is required from the authors or the publishers.

HOW TO CITE THIS ARTICLE

Tavakolpour, Y., Oloomi, S. A. A., Zare, M. H., Agha Mirjalily, S. A. & Mazidi, M. (2026). Numerical Investigation and Seasonal Optimization of a Phase-Change-Material-Integrated Solar Water Heating System. International Journal of Urban Management and Energy Sustainability, 7(3), 198–211.

DOI:10.22034/ijumes.2026.2108559.1419